Reflected Shock Tube Studies of High-Temperature Rate Constants for $CH_3 + O_2$, $H_2CO + O_2$, and $OH + O_2$

N. K. Srinivasan, M.-C. Su,† J. W. Sutherland,‡ and J. V. Michael*
Chemistry Division, Argonne National Laboratory, Argonne, Illinois 60439
Received: April 20, 2005; In Final Form: June 27, 2005

The reflected shock tube technique with multipass absorption spectrometric detection of OH-radicals at 308 nm, corresponding to a total path length of ∼2.8 m, has been used to study the reaction $CH_3 + O_2 \rightarrow CH_2O + OH$. Experiments were performed between 1303 and 2272 K, using ppm quantities of CH_3I (methyl source) and 5−10% O_2, diluted with Kr as the bath gas at test pressures less than 1 atm. We have also reanalyzed our earlier ARAS measurements for the atomic channel ($CH_3 + O_2 \rightarrow CH_3O + O$) and have compared both these results with other earlier studies to derive a rate expression of the Arrhenius form. The derived expressions, in units of cm^3 $molecule^{-1}$ s^{-1}, are $k = 3.11 \times 10^{-13}$ exp(−4953 K/T) over the *T*-range 1237−2430 K, for the OH-channel, and $k = 1.253 \times 10^{-11}$ exp(−14241*K*/*T*) over the *T*-range 1250−2430 K, for the O-atom channel. Since CH_2O is a major product in both reactions, reliable rates for the reaction $CH_2O + O_2 \rightarrow HCO + HO_2$ could be derived from $[OH]_t$ and $[O]_t$ experiments over the *T*-range 1587−2109 K. The combined linear least-squares fit result, $k = 1.34 \times 10^{-8}$ exp(−26883 K/T) cm^3 $molecule^{-1}$ s^{-1}, and a recent VTST calculation clearly overlap within the uncertainties in both studies. Finally, a high sensitivity for the reaction $OH + O_2 \rightarrow HO_2 + O$ was noted at high temperature in the O-atom data set simulations. The values for this obtained by fitting the O-atom data sets at later times (∼1.2 ms) again follow the Arrhenius form, $k = 2.56 \times 10^{-10}$ exp(−24145 K/T) cm^3 $molecule^{-1}$ s^{-1}, over the *T*-range, 1950−2100 K.

Introduction

The reaction of CH_3-radicals with O_2

$$CH_3 + O_2 \rightarrow \text{Products} \quad (1)$$

is one of the most important propagation reactions in the combustion chemistry of CH_4, and this has prompted experimental studies that span ∼55 years.[1] Three elementary reactions are possible[2]

$$CH_3 + O_2 (+M) \rightarrow CH_3O_2 (+M) \qquad \Delta H^\circ_{0,1a} = -30 \text{ kcal mol}^{-1} \quad (1a)$$

$$\rightarrow H_2CO + OH \qquad \Delta H^\circ_{0,1b} = -52 \text{ kcal mol}^{-1} \quad (1b)$$

$$\rightarrow CH_3O + O \qquad \Delta H^\circ_{0,1c} = 30 \text{ kcal mol}^{-1} \quad (1c)$$

reactions 1b and 1c can be viewed as forward dissociation paths from the initially formed and vibrationally hot methyl peroxy-radical with activation barriers that are higher lying than the entrance channel. As discussed by Zhu et al.,[2] eq 1a dominates at low temperature, but as temperature increases, eqs 1b and 1c become competitive with stabilization of the initially formed vibrationally hot peroxy radical. At the temperatures and relatively low pressures of the present experiments, eq 1a is expected to be negligible, with eqs 1b and 1c being the only important reactions.

Much of the earlier work on both channels was thoroughly reviewed by Yu et al.[3] In recent work from this laboratory,[4] the atomic channel, reaction 1c, was studied by atomic resonance absorption spectrometric (ARAS) detection of O-atoms. Our results agreed with modeling fits for eq 1c from the CH_4/O_2 branching chain oxidation experiments of Hwang et al.[5] but did not agree with similar experiments from Yu et al.[3] We found excessively large increases in [O] at relatively short times and therefore proposed a significance for the direct reaction

$$H_2CO + O_2 \rightarrow HCO + HO_2 \quad (2)$$

Both radical products from eq 2 rapidly dissociate at high *T* giving H-atoms that subsequently react with the large concentration of O_2 giving OH + O. In this O-atom study,[4] we did not find it necessary to invoke any significance for the molecular channel, eq 1b. The disagreement of rate constant values and the neglect of eq 1b prompted a comment from Eiteneer and Frenklach[6] and responses from Michael et al.[7] and Hwang et al.[8] Scire et al.[9] and Hessler et al.[10] have also indicated that their results cannot be explained without some significance for reaction 1b. The large spread in values for the branching ratio between eqs 1b and 1c,[3] along with the cited controversy,[6−10] motivated the recent shock tube study by Herbon et al.[11] who used both O-atom ARAS and OH-radical electronic absorption detection methods to assess the branching ratio. Between 1590 and 2430 K, their results for eq 1c were in good agreement with Hwang et al.[5] and were only 32% higher than those by Michael et al.[4] They did however find that eq 1b was the major process over their temperature range. The sum of both processes agreed with the results of Yu et al.[3]

* Corresponding author. Dr. J. V. Michael, D-193, Bldg. 200 Argonne National Laboratory Argonne, IL 60439, USA. Phone: (630) 252-3171. Fax: (630) 252-4470. E-mail: Michael@anlchm.chm.anl.gov.
† Faculty Research Participant, Department of Educational Programs, Argonne. Permanent address: Department of Chemistry, Butler University, Indianapolis, IN 46208.
‡ Present address: Guest Scientist, Department of Energy and Technology, Brookhaven National Laboratory, Upton, NY 11973.

10.1021/jp0581330 CCC: $30.25
Published on Web 08/12/2005

We earlier described a long absorption path multipass optical system for OH-radical detection in the reflected shock regime[12] and used it to measure other high-temperature rate constants.[13,14] Since the controversy[6−10] and new experimental results[11] have suggested that our earlier assertion[4] on the unimportance of eq 1b is incorrect, we have been motivated to study this reaction system again by directly observing OH-radical formation. In this work we have increased the path length for absorption by using 32 passes giving a total path length of 2.798 m,[14] as compared to 12 passes (1.049 m) in our earlier work.[13] Hence, a high sensitivity for OH-radical detection is possible thereby minimizing the effects of secondary reaction perturbations.

Experimental Section

The present experiments were performed with the shock tube technique using OH-radical electronic absorption detection. The method and the apparatus currently being used have been previously described,[15,16] and only a brief description of the experiment will be presented here.

The shock tube is constructed from 304 stainless steel in three sections. The first 10.2 cm o.d. cylindrical section is separated from the He driver chamber by a 4 mil unscored 1100-H18 aluminum diaphragm. A 0.25 m transition section then connects the first and third sections. The third section is of rounded corner (radius, 1.71 cm) square design and is fabricated from flat stock (3 mm) with a mirror finish. Two flat fused silica windows (3.81 cm) with broadband antireflection (BB AR) coating for UV light are mounted on the tube across from one another at a distance of 6 cm from the end plate. The path length between windows is 8.745 cm. The incident shock velocity is measured with eight fast pressure transducers (PCB Piezotronics, Inc., Model 113A21) mounted along the third portion of the shock tube, and temperature and density in the reflected shock wave regime are calculated from this velocity and include corrections for boundary layer perturbations.[17−19] The tube is routinely pumped between experiments to $<10^{-8}$ Torr by an Edwards Vacuum Products Model CR100P packaged pumping system. A 4094C Nicolet digital oscilloscope was used to record both the velocity and absorption signals.

The optical configuration consists of an OH resonance lamp, multipass reflectors, an interference filter at 308 nm, and a photomultiplier tube (1P28) all mounted external to the shock tube as described previously.[12−14,20] With this new configuration, a total path length of 2.798 m was obtainable thereby amplifying the measured absorbances by 32.

Gases. High purity He (99.995%), used as the driver gas, was from AGA Gases. Scientific grade Kr (99.999%), the diluent gas in reactant mixtures, was from Spectra Gases, Inc. The ~10 ppm impurities (N_2, 2 ppm; O_2, 0.5 ppm; Ar, 2 ppm; CO_2, 0.5 ppm; H_2, 0.5 ppm; CH_4, 0.5 ppm; H_2O, 0.5 ppm; Xe, 5 ppm; and CF_4, 0.5 ppm) are all either inert or in sufficiently low concentration so as to not perturb OH-radical profiles. The diluent gas also contained ~10% UHP He (99.999% from AGA Gases) in order to vibrationally relax O_2. Distilled water, evaporated at 1 atm into ultrahigh purity grade Ar (99.999%) from AGA Gases, was used at ~25 Torr pressure in the resonance lamp. Scientific grade O_2 (99.999%), for reaction mixtures, was obtained from MG Industries and was used without additional purification. Analytical grade CH_3I (99%) from Aldrich Chemical Co. Inc. was further purified by bulb-to-bulb distillations with the middle third being retained. Test gas mixtures were accurately prepared from pressure measurements using a Baratron capacitance manometer and were stored in an all glass vacuum line.

Results

In this study, $[OH]_t$ was determined from measured absorbance, $(ABS)_t = \ln[I_0/I_t] = [OH]_t l \sigma_{OH}$, through an earlier determination of the absorption cross section at 308 nm[14]

$$\sigma_{OH} = (4.516 - 1.18 \times 10^{-3}\, T) \times 10^{-17}\ \text{cm}^2\ \text{molecule}^{-1} \quad (3)$$

Equation 3 is accurate to ~±15%.

Fifty-four experiments were carried out with varying concentrations of both CH_3I and O_2 in 85%Kr−10%He diluent gas, and conditions are given in Table 1. Figure 1 shows three [OH] profiles at three different temperatures. With the present level of $[OH]_t$ and under the present conditions, simulations from a mechanism are therefore needed in order to determine rate constants for reaction 1b. We have expanded the mechanism used earlier[4] to include additional secondary reactions. Table 2 gives the mechanism along with rate constants taken from the literature; most of these reactions are known sufficiently well that they are not varied in the fitting procedure.

We first analyzed and modeled the new OH-radical data determining k_{1b}, and then the earlier O-atom data[4] were reanalyzed with tentative values for eq 1b, obtaining updated values for k_{1c}. In both analyses, we found it necessary to also vary k_2 in order to get agreement at longer times. In general, the initial concentration profiles for both OH-radicals and O-atoms were determined mostly by eqs 1b and 1c; however, under certain conditions, the determinations are highly coupled involving mutually fitting three rate constants in an iterative procedure between the two data sets. This situation can be addressed using sensitivity analysis as described below.

For the OH data, sensitivity analysis on the mechanism of Table 2 can be used to identify which reactions are important in determining $[OH]_t$. For the profile at 1303 K in Figure 1 and the other lower T experiments in Table 1, sensitivity analysis shows that only two reactions are important in determining $[OH]_t$, CH_3I dissociation and reaction 1b. Direct rate constant determinations on CH_3I have already been carried out in this laboratory,[21] and changing this rate constant by its uncertainty of ±35% gives only ~±20% changes in the k_{1b} value that fits the experiment. Hence, experiments at the lower temperatures in the table do give direct measurements of k_{1b}. At the intermediate temperatures near 1600 K in Table 1, only eleven processes contribute with the predominant process in the initial stages of reaction being eq 1b, as shown by the sensitivity analysis of Figure 2. At short times, there is slight sensitivity to CH_3I dissociation[21] and, at longer times, also from HO_2 dissociation.

Regarding HO_2 dissociation, the reverse reaction in seven bath gases including Kr was recently studied in this laboratory.[31] In that work, the relative collision efficiencies were determined, and new and existing third-order rate constant determinations were reviewed and fitted with a theoretical model. The values implied, from transformations through equilibrium constants, for HO_2 dissociation were within ±40−50% of earlier evaluations[22,52] that were based on less information. The success of the model for a variety of bath gases[31] leads us to prefer, over the present experimental temperature range, the transformed rate constant for $HO_2 + Kr$ listed in Table 2 (reaction 17 in the table). Hence, both reactions are well-known and cannot be significantly varied. Therefore, varying k_{1b} to simulate the experiments at short times gives values that are nearly direct, and the values obtained are listed in Table 1.

At longer times in this intermediate T-range (i.e., ~1600 K), where the $[OH]_t$ approaches a steady state, reaction 2 becomes the most important reaction, and this property allows rate constant estimates for $H_2CO + O_2$ to be made. The derived k_2

TABLE 1: High Temperature Rate Data for $CH_3 + O_2 \rightarrow CH_2O + OH$

P_1/Torr	M_s[a]	$\rho_5/(10^{18}$ cm$^{-3})$[b]	T_5/K[b]	k_{1b}	k_2
$X_{CH_3I} = 9.740 \times 10^{-6}$; $X_{O_2} = 4.988 \times 10^{-2}$; $X_{He} = 9.791 \times 10^{-2}$					
15.86	2.458	3.117	1456	9.59(−15)[c]	
15.87	2.419	3.068	1415	1.00(−14)	
15.97	2.568	3.268	1574	1.41(−14)	
15.91	2.462	3.126	1462	6.34(−15)	
15.86	2.411	3.051	1409	5.34(−15)	
15.92	2.377	3.028	1370	4.50(−15)	
10.92	2.493	2.185	1496	1.10(−14)	
10.95	2.351	2.052	1349	5.33(−15)	
10.93	2.433	2.131	1432	7.01(−15)	
10.96	2.420	2.125	1418	7.75(−15)	
10.88	2.429	2.114	1430	7.17(−15)	
10.90	2.438	2.133	1435	7.61(−15)	
10.90	2.332	2.024	1330	7.60(−15)	
$X_{CH_3I} = 4.851 \times 10^{-6}$; $X_{O_2} = 7.246 \times 10^{-2}$; $X_{He} = 1.045 \times 10^{-1}$					
10.89	2.355	2.079	1333	6.45(−15)	
10.87	2.325	2.044	1304	7.25(−15)	
10.90	2.375	2.101	1354	1.05(−14)	
10.91	2.454	2.181	1435	1.48(−14)	
10.91	2.420	2.147	1399	8.23(−15)	
10.90	2.420	2.145	1399	1.34(−14)	
10.93	2.649	2.365	1645	2.16(−14)	
15.93	2.515	3.254	1495	1.32(−14)	
15.81	2.559	3.284	1540	1.00(−14)	
15.92	2.358	3.042	1336	5.83(−15)	
15.82	2.337	2.993	1315	7.74(−15)	
15.86	2.420	3.115	1397	1.43(−14)	
15.90	2.500	3.229	1480	9.21(−15)	
15.91	2.383	3.074	1360	7.84(−15)	
15.97	2.324	3.003	1303	6.00(−15)	
$X_{CH_3I} = 1.695 \times 10^{-6}$; $X_{O_2} = 5.326 \times 10^{-2}$; $X_{He} = 9.526 \times 10^{-2}$					
15.98	2.352	3.002	1346	6.17(−15)	
15.91	2.522	3.209	1522	1.11(−14)	
15.94	2.415	3.080	1411	6.57(−15)	
15.91	2.548	3.241	1549	1.25(−14)	
15.88	2.523	3.205	1523	1.86(−14)	
15.90	2.323	2.948	1318	9.19(−15)	
15.99	2.479	3.172	1476	7.53(−15)	
$X_{CH_3I} = 1.819 \times 10^{-6}$; $X_{O_2} = 5.448 \times 10^{-2}$; $X_{He} = 9.743 \times 10^{-2}$					
10.85	2.794	2.421	1843	3.42(−14)	1.32(−14)
10.89	2.742	2.389	1780	2.94(−14)	4.62(−15)
10.86	2.862	2.474	1925	4.29(−14)	2.52(−14)
10.92	3.061	2.630	2178	4.27(−14)	
10.87	2.890	2.497	1959	2.64(−14)	2.61(−14)
10.91	3.132	2.674	2272	4.58(−14)	
10.92	3.064	2.632	2182	5.29(−14)	
10.89	2.686	2.343	1714	2.98(−14)	
10.84	2.891	2.492	1961	2.20(−14)	2.66(−14)
10.88	2.586	2.264	1596	1.94(−14)	
10.93	2.615	2.299	1628	2.14(−14)	2.35(−15)
15.96	2.579	3.281	1587	2.06(−14)	9.18(−16)
15.94	2.668	3.379	1685	3.20(−14)	1.42(−15)
15.92	2.640	3.332	1659	2.56(−14)	1.04(−15)
15.91	2.681	3.376	1705	2.90(−14)	
16.00	2.974	3.694	2052	2.63(−14)	5.71(−14)
15.89	3.126	3.803	2244	5.11(−14)	
15.99	2.920	3.642	1986	2.08(−14)	2.97(−14)
15.95	2.930	3.616	1965	1.78(−14)	2.20(−14)

[a] The error in measuring the Mach number, M_s, is typically 0.5−1.0% at the one standard deviation level. [b] Quantities with the subscript 5 refer to the thermodynamic state of the gas in the reflected shock region. [c] Parentheses denote the power of 10.

values are also listed in Table 1, but only for those experiments that gave superior profiles when extended to 1.5−2.0 ms. Data quality is always an issue as seen in Figure 1 where the signal-to-noise ratio is ∼5, entirely due to our decision to carry out the experiments at low [OH] in order to inhibit the effects of secondary reactions. Hence, the simulated k_{1b} and k_2 rate constants in Table 1 for $T = 1600 \pm 100$ K are estimated to only be accurate to ∼±20%.

Even though fewer reactions contribute, the experiments in Table 1 at high values of $T >$ ∼1750 K are more difficult to fit as indicated by the sensitivity analysis for 1986 K shown in Figure 3 where only seven reactions are sensitive. Reaction 1b still dominates in the initial stages, but both eqs 2 and 1c become increasingly important after about 100 μs. For $t >$ ∼400 μs, both $H_2CO \rightarrow H_2 + CO$ (reaction 19 in Table 2) and $OH + OH$ (reaction 12 in Table 2) show some significance.

H_2CO dissociation has been well characterized.[32] For the OH self-reaction, direct rate constants have been measured by Wooldridge et al.,[27] and these are consistent with $O + H_2O \rightarrow OH + OH$ transformed through equilibrium constants[15] using the recent re-evaluation for the heat of formation for OH-radicals.[24,25] Therefore, this reaction is likewise well characterized, and none of these rate constants can be varied.

With the present signal-to-noise ratio, there are unfortunately many combinations of the adjustable rates for eqs 1b, 1c, and 2 that can give acceptable fits. In this high T regime, we have reanalyzed our earlier O-atom results[4] (1665 K ≤ T ≤ 2109 K) with rate constants that are compatible with Arrhenius extrapolations of the $T <$ 1650 K results for eq 1b. From the O-atom profiles, new estimates for k_{1c} and also k_2 can be made, and this procedure and results are discussed in detail below. This is an iterative process (generally involving 2 to 3 iterations) between the two sets of data, [OH] and [O] profiles, and final iterations were carried out for each individual experiment in Table 1 at $T >$ 1750 K. The resulting values are also listed in the table for experiments that were considered to be of superior quality up to ∼2.0 ms. The fitting procedure involves simultaneous adjustment of two rates, namely, k_{1b} and k_2 with the reanalyzed k_{1c} values from the O-atom fits, and therefore, the final accuracy for k_{1b} at $T >$ 1750 K is ∼±30−40%. Note that eq 1c is so slow below 1650 K that it does not affect our conclusions at all on k_{1b} in the low T regime.

With the Table 1 values, an Arrhenius plot for reaction 1b is shown in Figure 4 along with a linear least squares line that includes all data points over the temperature range, 1303 to 2272 K. The line gives

$$k_{1b} = (8.36 \pm 2.47) \times 10^{-13} \times \exp(-6395 \pm 446 \text{ K/T}) \text{ cm}^3 \text{ molecule}^{-1} \text{ s}^{-1} \quad (4)$$

where the errors are one standard deviation values.

As mentioned above, the finding of a significant rate constant for eq 1b has required a reconsideration of our earlier O-atom data.[4] Figure 5 shows two experiments, one at 1665 K and the other at 1977 K, along with simulations using the mechanism of Table 2. The rate constants for eq 1b, as described by eq 4, were larger than those for eq 1c over the entire temperature range. Hence, in the final O-atom simulations, the rate constants for the molecular channel were fixed to the values implied by eq 4. At 1665 K, the sensitivity analysis shown in Figure 6 indicates that [O] is most sensitive to eq 1c as claimed earlier;[4] however, eqs 1b and 2 are also significant. The negative effect of eq 1b requires larger values for eq 1c than originally proposed. The values necessary to produce enough [O] at long times again implies some importance for eq 2, $H_2CO + O_2$.[4] Since H_2CO is produced from both processes, eqs 1b and 1c, the derived values for eq 2 are similar to those suggested in the earlier work.

As with the $[OH]_t$ fits for high temperatures, the O-atom profiles at high temperature are not straightforward, as seen in the sensitivity analysis in Figure 7 for the 1977 K experiment

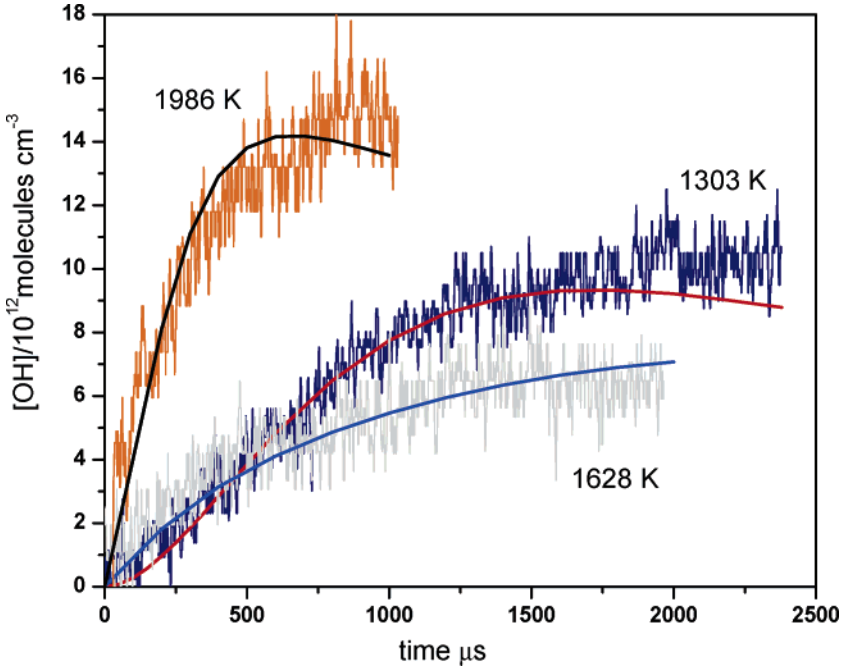

Figure 1. Three temporal profiles of [OH] measured at three different temperatures. (Solid lines) Fits with full reaction mechanism listed in Table 2. The conditions for the high-temperature profile are $P_1 = 15.99$ Torr and $M_s = 2.920$, $T_5 = 1986$ K, $\rho_5 = 3.642 \times 10^{18}$ molecules cm^{-3}, $[CH_3I]_0 = 6.624 \times 10^{12}$ molecules cm^{-3}, and $[O_2]_0 = 1.984 \times 10^{17}$ molecules cm^{-3}. The intermediate temperature conditions are $P_1 = 10.93$ Torr and $M_s = 2.615$, $T_5 = 1628$ K, $\rho_5 = 2.299 \times 10^{18}$ molecules cm^{-3}, $[CH_3I]_0 = 4.182 \times 10^{12}$ molecules cm^{-3}, and $[O_2]_0 = 1.253 \times 10^{17}$ molecules cm^{-3}. For the lowest temperature profile the conditions are $P_1 = 15.97$ Torr and $M_s = 2.324$, $T_5 = 1303$ K, $\rho_5 = 3.003 \times 10^{18}$ molecules cm^{-3}, $[CH_3I]_0 = 1.457 \times 10^{13}$ molecules cm^{-3}, and $[O_2]_0 = 2.176 \times 10^{17}$ molecules cm^{-3}.

of Figure 5. The most sensitive process at $t < 200$ μs is still eq 1c as claimed earlier.[4] However, reaction 2 followed by HO_2 dissociation (reaction 17 in Table 2) dominates in producing the excess [O], documented earlier,[4] after ~200−300 μs. As discussed above, even though reaction 1b, with the rate constant given by eq 4, contributes at low T, it is of minor significance at high T, partially corroborating our earlier decision to consider it to be negligible.[4] At high T, two other processes become important at longer times, namely, $H_2CO \rightarrow H_2 + CO$ (reaction 19 in Table 2)[32] and $OH + O_2 \rightarrow HO_2 + O$, the latter being postulated to explain the high levels of [O] produced at high temperatures in ~1.2 ms. Since HO_2 dissociation is well characterized,[31] three reactions (eqs 1c, 2, and 35 of Table 2) contribute strongly to the O-atom profiles at high temperatures requiring variation of all three reactions. Fortunately, the initial profiles are most strongly affected by eq 1c followed in time by eq 2 and then eq 35.

The values for eqs 1c and 2 derived from the fits are listed in Table 3, and an Arrhenius plot of the data for 1c is given in Figure 8. The upper line is from Yu et al.[3] As before,[4] it is still ~2−3 times too high. The lower line in the figure is from a linear-least-squares analysis of the data in the table and can be represented by

$$k_{1c} = (4.47 \pm 1.23) \times 10^{-12} \times \exp(-12572 \pm 522\ \mathrm{K/T})\ \mathrm{cm^3\ molecule^{-1}\ s^{-1}} \quad (5)$$

where the errors are one standard deviation values. We estimate the errors in k_{1c} to be ~±20−25%.[4] It should be noted that the values for eq 1c obtained by this procedure for both low and high T experiments were iteratively updated several times for use in the OH-radical analysis described above that gave the eq 4 result. This eq 4 result was likewise iteratively updated for use in the O-atom experiments giving eq 5.

Tables 1 and 3 list the rate constant values for reaction 2 that give acceptable fits for both the OH-radical and O-atom sets of data. As stated above, the values in Table 1 were obtained from $[OH]_t$ measurements at long times and, in Table 3, from O-atom measurements after about 100 to 200 μs up to ~700 to 900 μs depending on temperature. An Arrhenius plot of these values is shown in Figure 9. As seen in the figure, the two sets of data are scattered and overlap. We have used all points to determine a linear-least-squares line given by

$$\log k_2 = -(7.873 \pm 0.524) - (11675 \pm 981\ \mathrm{K})/T \quad (6)$$

where the errors are one standard deviation values, and the units of k_2 are cm^3 molecule^{-1} s^{-1}.

As noted above, it was necessary to postulate one additional reaction in the O-atom data set simulations at temperatures above ~1950 K. Simulations using only eqs 1b, 1c, and 2 were acceptable up to ~700−900 μs, but the predicted $[O]_t$ fell below the high-temperature experimental profiles at ~1 ms. We therefore postulate the importance of the reaction, $OH + O_2 \rightarrow HO_2 + O$ (reaction 35 in Table 2), at these high temperatures. This reaction is already present in simulations using well-known mechanisms[52,53] because the back reaction is included, and therefore, through equilibrium constants, the forward reaction is also included. The values for this reaction that are necessary to extend the O-atom simulations out to 1.2 ms follow the Arrhenius equation over the limited T-range, 1950−2100 K.

$$k_{35} = 2.56 \times 10^{-10} \exp(-24145\ \mathrm{K/T})\ \mathrm{cm^3\ molecule^{-1}\ s^{-1}} \quad (7)$$

Discussion

In this work, four rate constants have been estimated from two sets of data, and the results are summarized in eqs 4−7. The present findings show that rate constants for reaction 1b

TABLE 2: Mechanism for Fitting [O] and [OH] Profiles from the $CH_3 + O_2$ Reaction[a]

1b	$CH_3 + O_2 \rightarrow H_2CO + OH$	k_{1b} = to be fitted	
1c	$CH_3 + O_2 \rightarrow CH_3O + O$	k_{1c} = to be fitted	
2	$H_2CO + O_2 \rightarrow HCO + HO_2$	k_2 = to be fitted	
3	$CH_3I + Kr \rightarrow CH_3 + I + Kr$	$k_3 = 8.04 \times 10^{-9} \exp(-20\,566\ K/T)$	[21]
4	$CH_3O + Kr \rightarrow H_2CO + H + Kr$	$k_4 = 6.51 \times 10^{13}\, T^{-6.65} \exp(-16\,704\ K/T)$	[22]
5	$H + O_2 \rightarrow OH + O$	$k_5 = 1.62 \times 10^{-10} \exp(-7474\ K/T)$	[23]
6	$OH + O \rightarrow O_2 + H$	$k_6 = 5.42 \times 10^{-13}\, T^{0.375} \exp(950\ K/T)$	[15,24,25]
7	$O + H_2 \rightarrow OH + H$	$k_7 = 8.44 \times 10^{-20}\, T^{2.67} \exp(-3167\ K/T)$	[15]
8	$OH + H \rightarrow H_2 + O$	$k_8 = 3.78 \times 10^{-20}\, T^{2.67} \exp(-2393\ K/T)$	[15,24,25]
9	$OH + H_2 \rightarrow H_2O + H$	$k_9 = 3.56 \times 10^{-16}\, T^{1.52} \exp(-1736\ K/T)$	[26]
10	$H_2O + H \rightarrow OH + H_2$	$k_{10} = 1.56 \times 10^{-15}\, T^{1.52} \exp(-9083\ K/T)$	[15,24,25]
11	$O + H_2O \rightarrow OH + OH$	$k_{11} = 7.48 \times 10^{-20}\, T^{2.7} \exp(-7323\ K/T)$	[15,24,25]
12	$OH + OH \rightarrow O + H_2O$	$k_{12} = 7.19 \times 10^{-21}\, T^{2.7} \exp(917\ K/T)$	[15,24,25,27]
13	$H_2CO + OH \rightarrow H_2O + HCO$	$k_{13} = 5.69 \times 10^{-15}\, T^{1.18} \exp(225\ K/T)$	[28]
14	$H_2CO + O \rightarrow OH + HCO$	$k_{14} = 6.92 \times 10^{-13}\, T^{0.57} \exp(-1390\ K/T)$	[28]
15	$HCO + Kr \rightarrow H + CO + Kr$	$k_{15} = 6.0 \times 10^{-11} \exp(-7722\ K/T)$	[29]
16	$HCO + O_2 \rightarrow HO_2 + CO$	$k_{16} = 1.26 \times 10^{-11} \exp(-204\ K/T)$	[30]
17	$HO_2 + Kr \rightarrow H + O_2 + Kr$	$k_{17} = 7.614 \times 10^{-10} \exp(-22\,520\ K/T)$	[31]
18	$H_2CO + Kr \rightarrow HCO + H + Kr$	$k_{18} = 1.019 \times 10^{-8} \exp(-38\,706\ K/T)$	[32]
19	$H_2CO + Kr \rightarrow H_2 + CO + Kr$	$k_{19} = 4.658 \times 10^{-9} \exp(-32\,110\ K/T)$	[32]
20	$I + O_2 \rightarrow IO + O$	$k_{20} = 7 \times 10^{-11} \exp(-30\,977\ K/T)$	[4]
21	$CH_3 + CH_3 \rightarrow C_2H_6$	$k_{21}(\rho,T)$	[33−35]
22	$CH_3 + CH_3 \rightarrow C_2H_4 + 2H$	$k_{22} = 5.26 \times 10^{-11} \exp(-7392\ K/T)$	[36]
23	$O + C_2H_6 \rightarrow OH + H + C_2H_4$	$k_{23} = 1.87 \times 10^{-10} \exp(-3950\ K/T)$	[37]
24	$OH + C_2H_4 \rightarrow H_2O + H + C_2H_2$	$k_{24} = 3.35 \times 10^{-11} \exp(-2990\ K/T)$	[38]
25	$CH_3 + O \rightarrow H_2CO + H$	$k_{25} = 1.148 \times 10^{-10}$	[39,40]
26	$CH_3 + O \rightarrow H_2 + CO + H$	$k_{26} = 2.52 \times 10^{-11}$	[39,40]
27	$CH_3 + OH \rightarrow {}^1CH_2 + H_2O$	$k_{27} = 1.15 \times 10^{-9}\, T^{-0.4884}$	[41]
28	${}^1CH_2 + Kr \rightarrow CH_2 + Kr$	$k_{28} = 4.0 \times 10^{-14}\, T^{0.93}$	[42,43]
29	${}^1CH_2 + O_2 \rightarrow CH_2 + O_2$	$k_{29} = 5.2 \times 10^{-11}$	[44,45]
30	$CH_2 + O_2 \rightarrow H_2CO + O$	$k_{30} = 6.56 \times 10^{-12} \exp(-750\ K/T)$	[46,47]
31	$CH_2 + O_2 \rightarrow CO_2 + 2H$	$k_{31} = 8.61 \times 10^{-12} \exp(-750\ K/T)$	[46,47]
32	$CH_2 + O_2 \rightarrow CO_2 + H_2$	$k_{32} = 7.80 \times 10^{-12} \exp(-750\ K/T)$	[46,47]
33	$CH_2 + O_2 \rightarrow HCO + OH$	$k_{33} = 1.394 \times 10^{-11} \exp(-750\ K/T)$	[46,47]
34	$OH + HO_2 \rightarrow O_2 + H_2O$	$k_{34} = 2.35 \times 10^{-10}\, T^{-0.21} \exp(56\ K/T)$	[48]
35	$OH + O_2 \rightarrow HO_2 + O$	k_{35} = see text	
36	$OH + C_2H_6 \rightarrow C_2H_4 + H_2O + H$	$k_{36} = 2.68 \times 10^{-18}\, T^{2.224} \exp(-373\ K/T)$	[49]
37	$CH_3OH + Kr \rightarrow CH_3 + OH + Kr$	$k_{37} = 1.10 \times 10^{-7} \exp(-33\,100\ K/T)$	[41]
38	$OH + CH_3OH \rightarrow H_2CO + H_2O + H$	$k_{38} = 1.10 \times 10^{-19}\, T^{2.5} \exp(483\ K/T)$	[50]
39	$H_2 + O_2 \rightarrow H + HO_2$	$k_{39} = 1.228 \times 10^{-18}\, T^{2.43} \exp(-26\,926\ K/T)$	[51]

[a] All rate constants are in cm^3 molecule^{-1} s^{-1}.

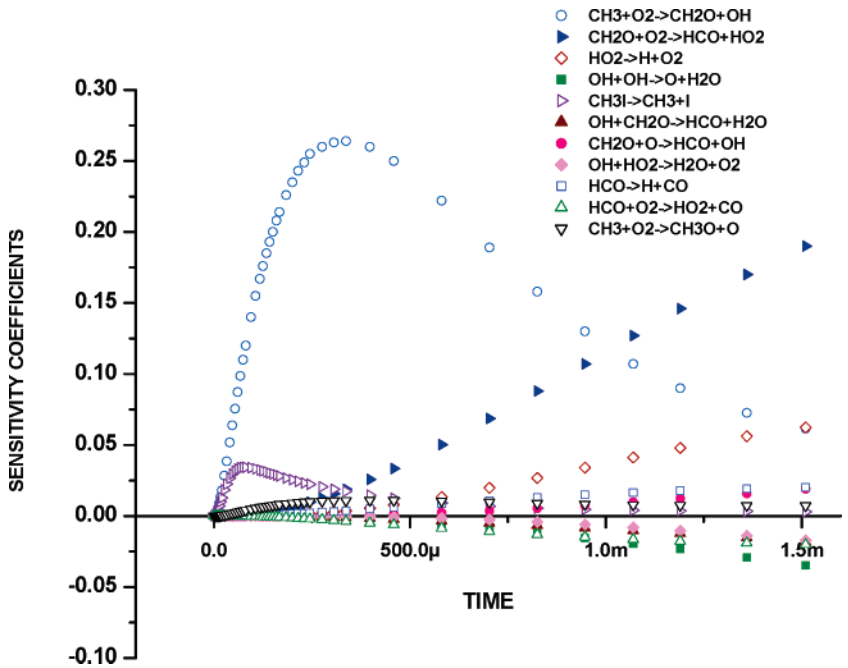

Figure 2. OH-radical sensitivity analysis for the 1628 K profile shown in Figure 1 using the full reaction mechanism scheme and the final fitted values for k_{1b} and k_2 listed in Table 1. The eleven most sensitive reactions are shown.

are larger than those for eq 1c over the entire temperature range, contradicting our original assertion.[4] In the paragraphs to follow, the present results are compared to earlier determinations and to existing theoretical studies.

$CH_3 + O_2 \rightarrow H_2CO + OH$: The earlier data on reaction 1b have been thoroughly reviewed.[1,3,11] As pointed out by Yu et al.,[3] the published results prior to 1995 fall into one of two groups. The theoretical estimate of Zellner and Ewig[54] is a lower

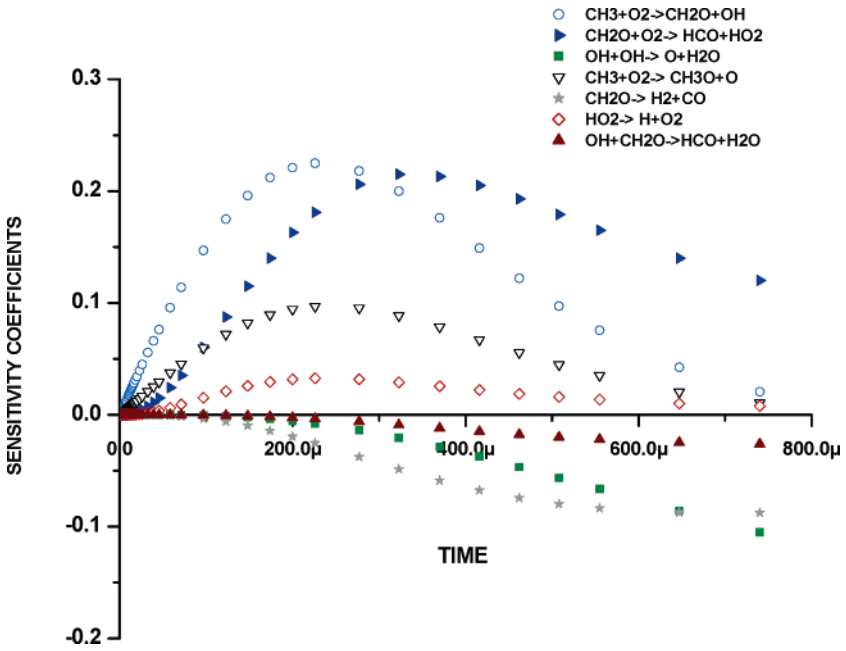

Figure 3. OH-radical sensitivity analysis for the 1986 K profile shown in Figure 1 using the full reaction mechanism scheme and the final fitted values for k_{1b} and k_2 listed in Table 1. The seven most sensitive reactions are shown.

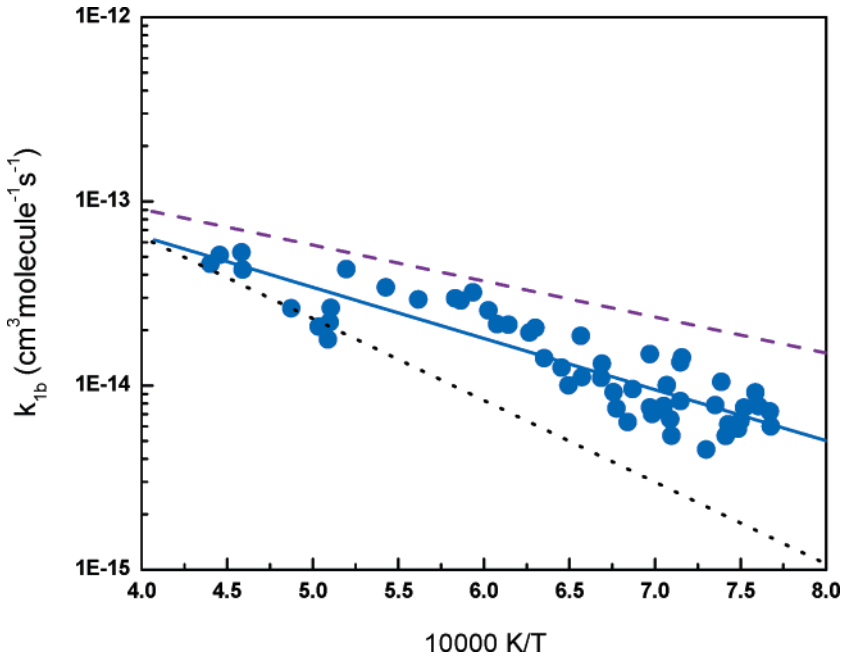

Figure 4. Arrhenius plot of the data for k_{1b} from Table 1. (●) Present work (1303−2272 K). (Solid blue line) Fit to the present data (eq 4 in text), (dotted line) ref 52, and (purple dashed line) ref 53.

boundary for the "high" group that includes approximately 10 earlier studies. The Leeds Methane Mechanism[53] has preferred to use a slightly modified Zellner and Ewig value for this rate constant. On the other hand, Yu et al. used theory and sensitivity analysis to inform their choice of values for fitting branched chain oxidation studies of CH_4, and their final values are representative of the "low" group. The extrapolated values from Yu et al. are slightly modified in the popular kinetics code for methane oxidation, GRI Mech.[52] The result is about an order of magnitude discrepancy at lower temperatures between the Leeds and GRI mechanisms for this rate constant. The results from these earlier evaluations are shown in Figure 4 along with the present values where the summary, eq 4, is between the high and low groups.

To develop an evaluated rate constant from measurements that span many decades and are of uneven quality, decisions have to be made on which studies to include in the evaluation. In the past 10 years, there have been four experimental studies[3,10,11,55] on reaction 1b besides our own. One of these is the Yu et al.[3] study that falls into the "low" group, as discussed above. Another is the unpublished thesis dissertation study by Naumann,[55b] which was partially reported by Braun-Unkhoff et al.[55a] The final results[55b] of this fall into the "high" group. The other two studies,[10,11] like the present, fall between these two groups. We believe that this most recent ten-year record is a reasonable basis for an evaluation whose details are now described below.

Between 1550 and 2200 K, Yu et al.[3] report a value for eq 1b of

$$k_{1b} = 3.072 \times 10^{-12} \exp(-10224\ \mathrm{K/T})\ \mathrm{cm^3\ molecule^{-1}\ s^{-1}} \quad (8)$$

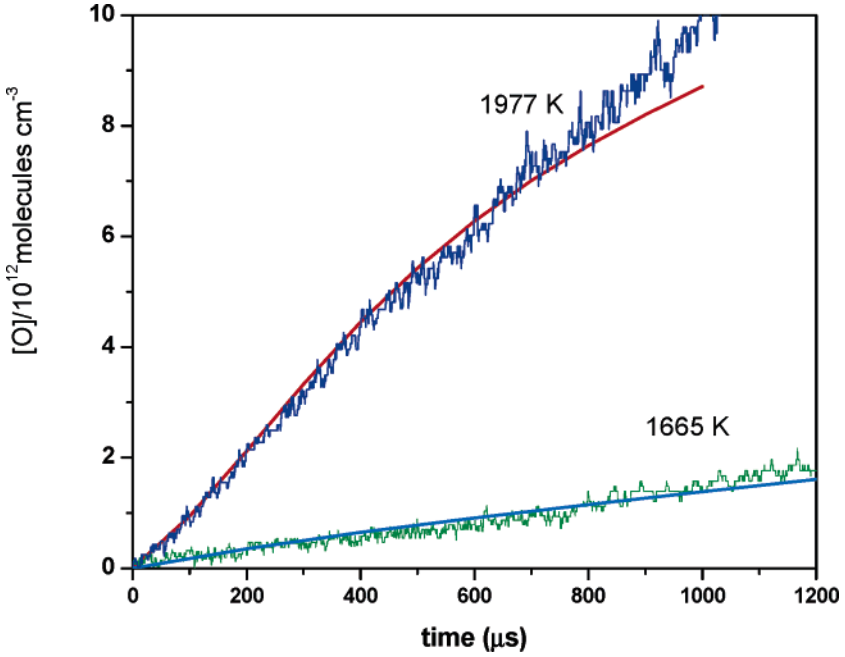

Figure 5. Measured O-atom profiles for two typical experiments. (Solid lines) Fits with full reaction mechanism listed in Table 2. The conditions for the upper trace are $P_1 = 10.95$ Torr and $M_s = 2.909$, $T_5 = 1977$ K, $\rho_5 = 2.539 \times 10^{18}$ molecules cm^{-3}, $[CH_3I]_0 = 4.042 \times 10^{12}$ molecules cm^{-3}, and $[O_2]_0 = 1.478 \times 10^{17}$ molecules cm^{-3}. The conditions for the lower trace are $P_1 = 10.99$ Torr and $M_s = 2.647$, $T_5 = 1665$ K, $\rho_5 = 2.340 \times 10^{18}$ molecules cm^{-3}, $[CH_3I]_0 = 3.725 \times 10^{12}$ molecules cm^{-3}, and $[O_2]_0 = 1.362 \times 10^{17}$ molecules cm^{-3}.

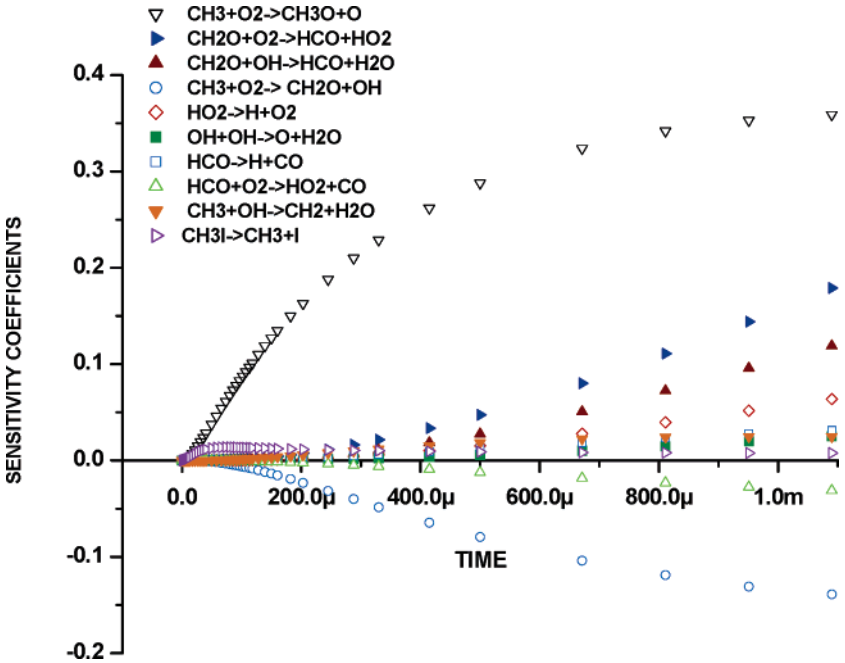

Figure 6. O-atom sensitivity analysis for the 1665 K profile shown in Figure 5 using the full reaction mechanism scheme and the final fitted values for k_{1c} and k_2 listed in Table 3. The ten most sensitive reactions are shown.

Equation 8 was determined by fitting induction period data to a complex mechanism using sensitivity analysis to determine the best experimental conditions. Equation 8 is plotted along with the summary of the present data, eq 4, in Figure 10.

Hessler et al.[10] have determined rate constants using the tunable-laser flash-absorption technique[56] to observe OH-radicals directly behind incident shock waves. These experiments used $(CH_3)_2N_2$ as the source of CH_3-radicals in the presence of ~30% O_2 in Ar bath gas. Large quantities of He and/or CF_4 were additionally added to vibrationally relax O_2. The sensitivity spectrum with such large concentrations is entirely different than that in the present work. Even so, these workers were able to design experiments where reaction 1b was the significant methyl depletion reaction. The weighted least-squares fit to their data is

$$k_{1b} = 1.24 \times 10^{-12} \exp(-7172\ \mathrm{K/T})\ \mathrm{cm^3\ molecule^{-1}\ s^{-1}} \quad (9)$$

over the temperature range 1237 to 1520 K. Even though this and the present experiments have used the same diagnostic, the experiments are not identical. The present work utilizes very low $[CH_3]_0$ and observes $[OH]_t$ for long times up to 2 ms, whereas the laser flash absorption method uses very high $[CH_3]_0$ and observes $[OH]_t$ for particle times <50 μs. Equation 9 is also plotted in Figure 10 where the agreement between eqs 4 and 9 is seen to be excellent.

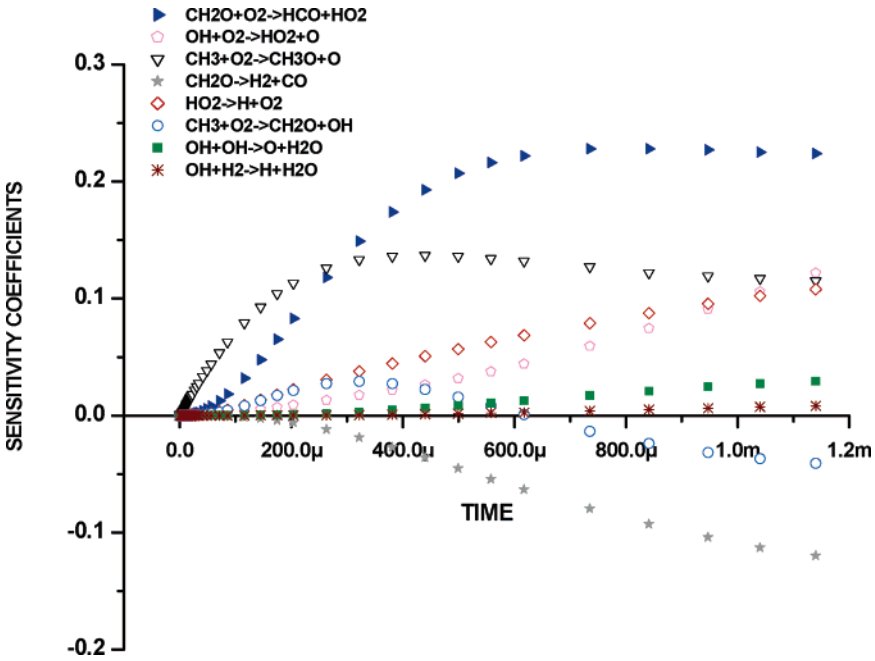

Figure 7. O-atom sensitivity analysis for the 1977 K profile shown in Figure 5 using the full reaction mechanism scheme and the final fitted values for k_{1c} and k_2 listed in Table 3. The eight most sensitive reactions are shown.

TABLE 3: High Temperature Rate Data for $CH_3 + O_2 \rightarrow CH_3O + O$

P_1/Torr	M_s[a]	$\rho_5/(10^{18}$ cm$^{-3})$[b]	T_5/K[b]	k_{1c}	k_2
$X_{CH_3I} = 2.482 \times 10^{-6}$; $X_{O_2} = 1.056 \times 10^{-1}$					
5.96	2.823	1.410	1802	4.39(−15)[c]	3.49(−15)
5.92	3.055	1.502	2078	1.09(−14)	2.32(−14)
7.48	2.959	1.847	1962	7.02(−15)	1.13(−14)
7.46	3.045	1.887	2066	1.01(−14)	1.92(−14)
$X_{CH_3I} = 1.592 \times 10^{-6}$; $X_{O_2} = 5.822 \times 10^{-2}$					
10.96	2.865	2.517	1916	7.06(−15)	9.76(−15)
10.79	2.998	2.574	2083	1.09(−14)	5.47(−14)
10.95	3.018	2.626	2109	1.18(−14)	3.56(−14)
10.99	2.960	2.594	2035	8.86(−15)	1.84(−14)
10.93	2.824	2.479	1867	6.07(−15)	5.03(−15)
10.91	2.688	2.357	1712	2.99(−15)	1.09(−15)
10.97	2.715	2.392	1744	3.58(−15)	1.56(−15)
10.99	2.647	2.340	1665	2.19(−15)	7.47(−16)
10.98	2.776	2.444	1815	3.61(−15)	1.66(−15)
10.95	2.909	2.539	1977	7.34(−15)	1.37(−14)
10.93	2.971	2.579	2055	9.07(−15)	2.34(−14)
10.93	2.999	2.599	2091	1.12(−14)	1.55(−14)

[a] The error in measuring the Mach number, M_s, is typically 0.5−1.0% at the one standard deviation level. [b] Quantities with the subscript 5 refer to the thermodynamic state of the gas in the reflected shock region. [c] Parentheses denote the power of 10.

In work similar to the present, Herbon et al.[11] observed both $[OH]_t$ and $[O]_t$ using electronic absorption and ARAS methods, respectively. These reflected shock wave experiments in Ar used CH_3I as the source of $[CH_3]_0$,with high $[O_2]$ and [He], and were carried out at somewhat higher pressures. In general, [OH] was ∼5−20 times higher than that in the present work. From normalized $[OH]_t$ measurements, they were able to determine the total rate constant $k_1 = k_{1b} + k_{1c}$, where the k_{1c} values were determined from the O-atom results. In the fitting procedure, the branching ratio $\alpha = k_{1c}/k_1$ was evaluated, allowing a rate constant expression to be specified for eq 1b,

$$k_{1b} = 1.14 \times 10^{-22}\, T^{2.86} \times \exp(-4916\ \text{K/T})\ \text{cm}^3\ \text{molecule}^{-1}\ \text{s}^{-1} \quad (10)$$

over the temperature range 1590 to 2430 K. The A-factor and T-dependence was chosen to be identical to the theoretical results of Zhu et al.[2] Equation 10 is also plotted in Figure 10 and can be compared to the present results and those from Yu et al. and Hessler et al., as summarized by eqs 4, 8, and 9, respectively.

The final study is from Stuttgart where OH was observed by narrow bandwidth laser absorption, and both O- and H-atoms were observed by the ARAS technique.[55] Rate constants were obtained by fitting a mechanism with variable values for both channels. The earlier[55a] was subsequently updated with more extensive analyses,[55b] and the preferred result for eq 1b is now

$$k_{1b} = 2.906 \times 10^{-12} \exp(-7000\ \text{K/T})\ \text{cm}^3\ \text{molecule}^{-1}\ \text{s}^{-1} \quad (11)$$

over the temperature range 1250 to 1600 K. The activation energy chosen for eq 11 was from a calculation by Walch,[57] and the value for the A-factor was determined from fits to the data. Equation 11 is also plotted in Figure 10 along with the other results. Clearly, the extrapolated results from eqs 4, 8, 9, and 10 all agree, within experimental error, above 2000 K; however, the extrapolated results from eq 11 diverge from the other sets at high temperatures.

Equations 4, 8, 9, 10, and 11 have been used to generate a database over the temperature range, 1237−2430 K, by calculating five equally spaced points in T^{-1}, but only over the T-range of a given study. Each study therefore has equal weight. The resulting 25 points are fitted with the Arrhenius expression, and the least-squares result is

$$k_{1b} = 3.11 \times 10^{-13} \exp(-4953\ \text{K/T})\ \text{cm}^3\ \text{molecule}^{-1}\ \text{s}^{-1} \quad (12)$$

for 1237−2430 K. Equation 12 is then an evaluation and is compared to the studies in Figure 10 where it is plotted as the thick solid line. Except for the highest temperature point by Herbon et al.,[11] eq 12 is within ∼±46% of the present work and two of the studies[10,11] that were used to derive it, being closest to the results of Hessler et al.[10] The results of Yu et al.[3] and Naumann[55b] are low and high, respectively, by up to a factor of 3.

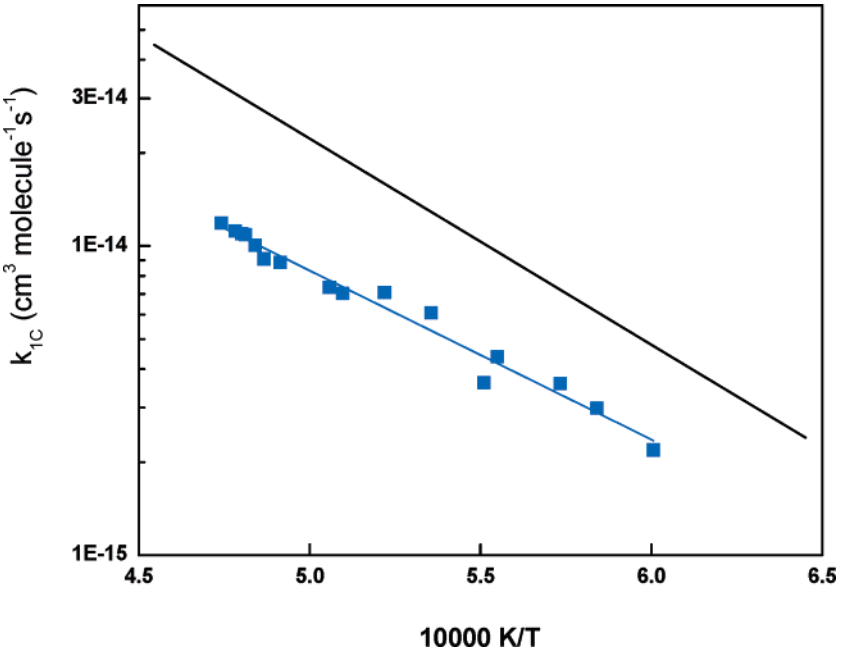

Figure 8. Arrhenius plot of the data for k_{1c} from Table 3. (■) Present work (1665−2109 K). (Thin solid blue line) Linear least-squares fit that includes all data points (eq 5 in text), (thick solid line) ref 3.

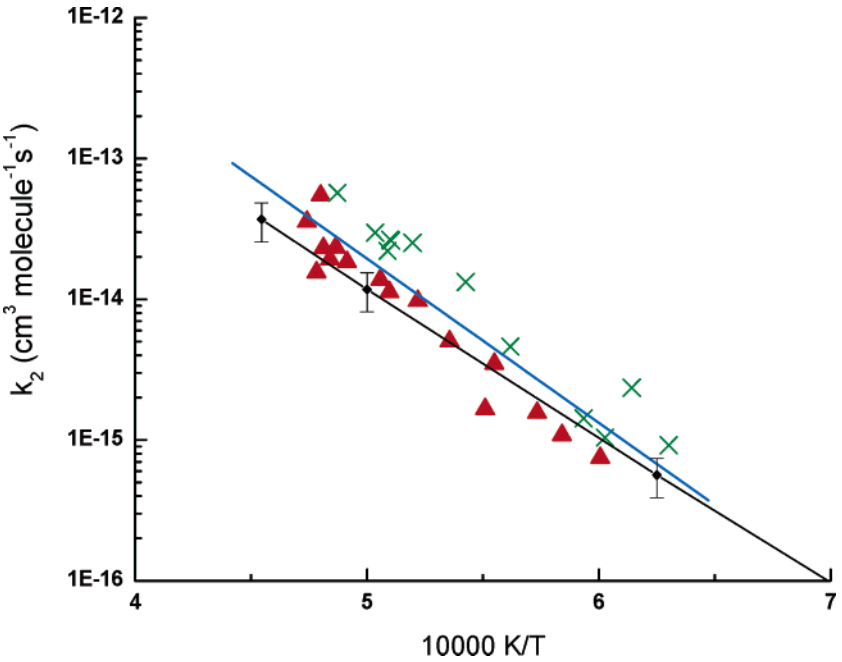

Figure 9. Arrhenius plot of the data for k_2. (×) Values listed in Table 1 (see text). (▲) Values listed in Table 3 (see text). (Solid blue line) Linear-least-squares fit that includes the crosses and the triangles (eq 6 in text). (Solid black line) Variational transition state theoretical calculation with error bars (see text).

Zhu et al.[2] have carried out ab initio electronic structure calculations on eq 1b, determining transition state and reactant structures. They also found the crossing point between $^2A'$ and $^2A''$ states. The lowest barrier was calculated to be 15.0 kcal mol^{-1}. Presuming that the probability for state crossing was unity, they then carried out microcanonical variational transition state RRKM theoretical calculations to estimate k_{1b}. At 1 atm and 1000 K ≤ T ≤ 3000 K, they reported $k_{1b} = 1.14 \times 10^{-22}$ $T^{2.86}$ exp(−5115 K/T) cm^3 $molecule^{-1}$ s^{-1}. This expression predicts values that agree with eq 12 within experimental error at high temperature but, at lower temperatures, diverges to values that are three to four times lower. Changing the apparent activation energy to 4292 K (8.529 kcal mol^{-1}) gives the compromise value shown as the green line in Figure 10. This suggests that the barrier could be ∼1.6 kcal mol^{-1} lower than that suggested by Zhu et al. at 13.4 kcal mol^{-1}, in better agreement with an earlier estimate of 13.7 kcal mol^{-1} by Walch.[57]

$CH_3 + O_2 \rightarrow CH_3O + O$: The earlier data on reaction 1c have been thoroughly reviewed,[1−5] and the spread in values is substantially less than that for reaction 1b. The line summarizing the present results, eq 5, is plotted in Figure 11. In the past decade, there are four additional studies[3,5,11,55] to which the present reanalysis can be compared. Hwang et al.,[5] Herbon et al.,[11] and Naumann[55b] have reported respective values of

$$k_{1c} = 2.66 \times 10^{-11} \exp(-15813\ \text{K/T})\ (1575-1822\ \text{K}) \quad (13)$$

$$k_{1c} = 1.01 \times 10^{-16} T^{1.54} \exp(-14005\ \text{K/T})\ (1590-2430\ \text{K}) \quad (14)$$

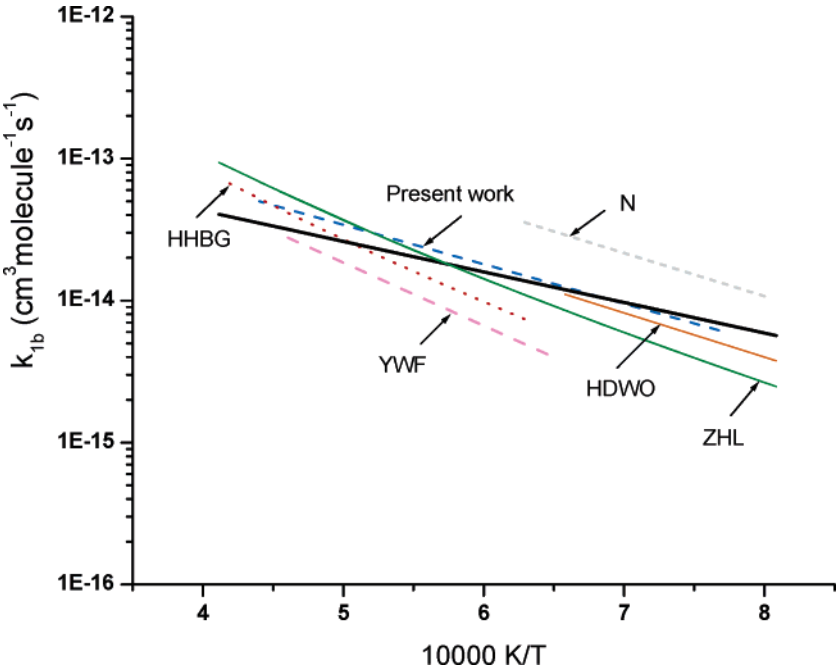

Figure 10. Comparison of the present work with recent experimental and predicted results for k_{1b}. (Dashed blue line) Present work (eq 4 in text), (YWF) ref 3 (eq 8 in text), (HDWO) ref 10 (eq 9 in text), (HHBG) ref 11 (eq 10 in text), and (N) ref 55b (eq 11 in text). The thick solid line is a linear-least-squares fit (eq 12 in text), and ZHL (ref 2) is a modified theoretical expression (see text).

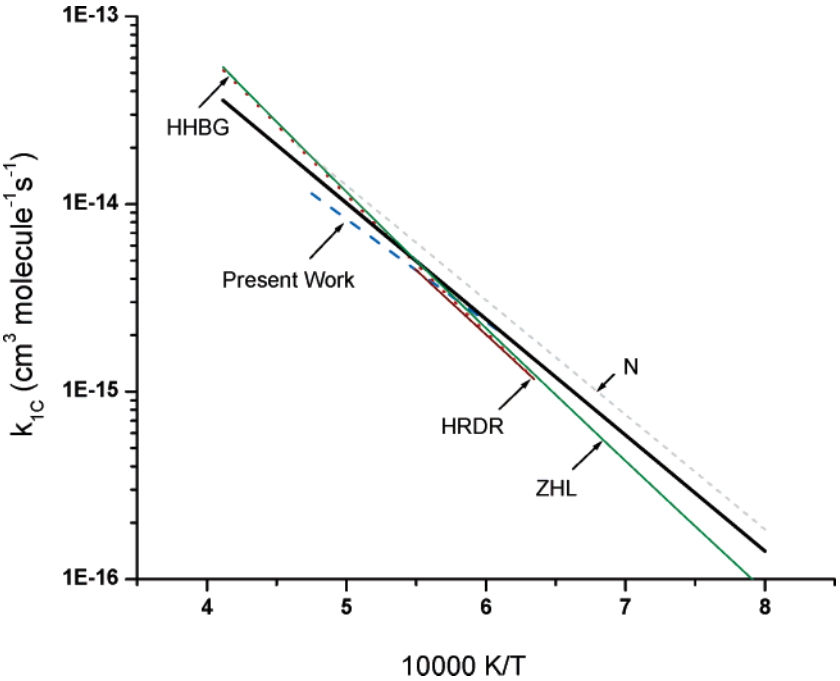

Figure 11. Comparison of the present work with recent experimental results for k_{1c}. (Dashed line) Present work (eq 5 in text), (HRDR) ref 5 (eq 13 in text), (HHBG) ref 11 (eq 14 in text), and (N) ref 55b (eq 15 in text). The thick solid line is a linear-least-squares fit (eq 16 in text), ZHL (ref 2) is a modified theoretical expression (see text).

and

$$k_{1c} = 1.428 \times 10^{-11} \exp(-14070\ \text{K/T})\ (1250-2150\ \text{K}) \quad (15)$$

all in cm^3 molecule^{-1} s^{-1}. The fourth study, Yu et al.,[3] gives a result that is substantially higher than those eqs 5 and 13−15. The present result, eq 5, and these studies have been used to generate a database over the temperature range, 1250−2430 K. Five points are calculated from the expressions over equal ranges in T^{-1} but only over the T-range of a given study. Hence, each study is given equal weight. The results of Yu et al.,[3] being higher than eqs 5 and 13−15, have therefore not been included in the database. The resulting 20 points are then fitted to the Arrhenius equation, and the least-squares result for 1250−2430 K is

$$k_{1c} = 1.253 \times 10^{-11} \exp(-14241\ \text{K/T})\ \text{cm}^3\ \text{molecule}^{-1}\ \text{s}^{-1} \quad (16)$$

Equation 16 is then an evaluation based on four studies. Values from these studies are calculated to be within $<\pm 30\%$ from eq

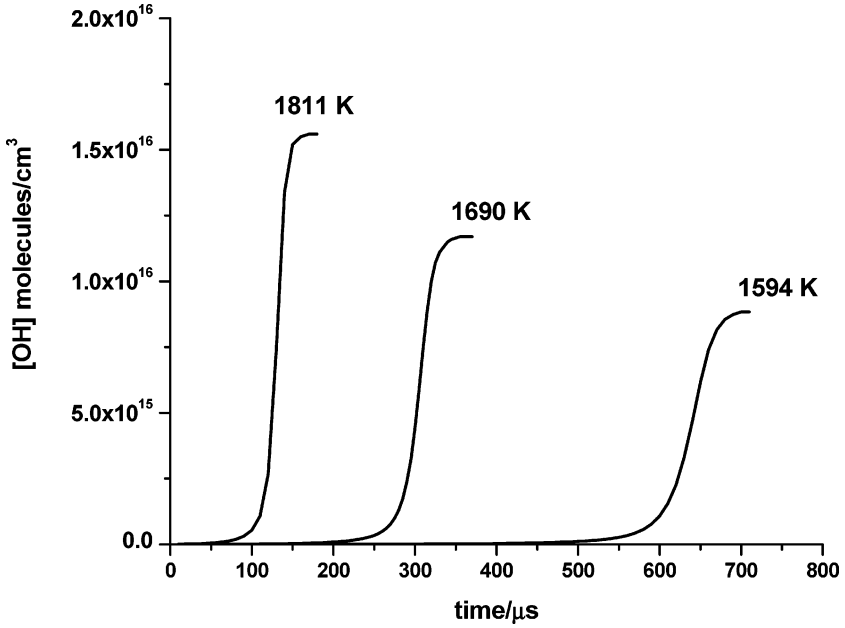

Figure 12. A simulation of OH profiles at three temperatures 1811, 1690, and 1594 K, respectively, using the mechanism of Table 2 and the evaluated rate constants for k_{1b} (eq 12 in text), k_{1c} (eq 16 in text), k_2 (eq 6 in text), and k_{35} (eq 7 in text). The total densities are 1.060×10^{19}, 1.018×10^{19}, and 9.877×10^{18} molecules cm^{-3}, respectively, for 0.5% CH_4 and 10% O_2 mixtures.

16 except for the 2430 K value from Herbon et al.[11] It should be pointed out that this level of error is close to those reported in the original studies. The rate expressions for eq 1c used in the mechanisms GRI Mech[52] and the Leeds Methane Mechanism[53] are both ~2.5−3.0 times too high, and therefore, eq 16 should be used for the atomic channel.

Zhu et al. have also carried out ab initio electronic structure calculations on eq 1c,[2] determining transition state and reactant structures. In this case, the reaction occurs on the $^2A''$ surface. The barrier height used in their RRKM calculations was 28.8 kcal mol^{-1}, and there is no barrier for the reverse reaction. Again using flexible variational transition state theory, the rate constant calculated for 1c at 1 atm and 1000 K ≤ T ≤ 3000 K is $k_{1c} = 1.01 \times 10^{-16}\ T^{1.54} \exp(-13276\ \text{K/T})$ cm^3 molecule^{-1} s^{-1}. This expression predicts values that are nearly equal to eq 16 at 1250 K but diverge to a value nearly two times higher at 2430 K. As seen in Figure 11, by raising the apparent activation energy to 13920 K (27.663 kcal mol^{-1}), the adjusted theoretical values are within ±30% of eq 16 over most of the temperature range, diverging to ±40−50% at the highest and lowest temperatures in the database used to derive eq 16. This would then suggest that the barrier height might be 1.3 kcal mol^{-1} higher, at 30.1 kcal mol^{-1}, than that used by Zhu et al. This higher value agrees with two recent thermochemical evaluations of 29.9 ± 0.5[58] and 29.8 ± 0.1[59] kcal mol^{-1} by Ruscic et al. and Ruscic, respectively, who now prefer $\Delta_f H^\circ_{0,CH_3O} = 6.63 \pm 0.10$ kcal mol^{-1} using active tables instead of the 5.4 kcal mol^{-1} used by Zhu et al.

$H_2CO + O_2 \rightarrow HCO + HO_2$: As stated above, both the $[OH]_t$ and $[O]_t$ experiments allow rate constant estimates for reaction 2, and the values obtained (Tables 1 and 3) are plotted in Figure 9. Direct values based on O-atom ARAS experiments have also been carried out in this laboratory, and variational transition state theoretical estimates of thermal rate constants for the reverse reaction have been made using an unscaled potential energy surface calculation.[60] The transition state is loose and has two hindered rotors. Theoretical rate constants for the reaction are then calculated from the backward rates coupled to updated equilibrium constant values from active tables.[58,59] The rate constant estimates show substantial Arrhenius plot curvature and cannot be appropriately expressed using the usual Arrhenius expression. However, the theoretical results can be expressed to within ±2% by the three-parameter expression

$$k_2 = 2.35 \times 10^{-20}\ T^{2.9754} \times \exp(-18984\ \text{K/T})\ \text{cm}^3\ \text{molecule}^{-1}\ \text{s}^{-1} \quad (17)$$

over the temperature range 500−2400 K. Because of a spread in calculated barrier values depending on the choice of the electronic structure method, eq 17 is only accurate to ±30% over the temperature range. This spread of values is shown in Figure 9 along with the line calculated from eq 17. If eqs 6 and 17 are compared, eq 17 is lower than eq 6 by ~15−40% over the present T-range, and therefore, theory and experiment do overlap within the range of uncertainties in both.

$OH + O_2 \rightarrow HO_2 + O$: As stated above, this postulated reaction (reaction 35 in Table 2) was important in fitting $[O]_t$ at high temperature with the necessary rate constant given by eq 7. The reverse reaction (eq −35) shows a slight negative T-dependence in the 200−350 K regime.[1] There is only one high temperature estimate for eq 35,[1] and therefore, almost nothing is known about this reaction. Theoretical electronic structure calculations on the HO_3 system have been carried out,[61,62] and a negligible barrier for eq −35 is predicted, in agreement with the small measured T-dependence. The Varandas et al. calculations[62] suggest that eq −35 goes through an H-bonded structure (at 1.35 kcal mol^{-1} below separated reactants) before proceeding down the steep well toward products OH + O_2. An upper limit can be estimated using the collision rate constant for eq −35 with methods described earlier[63] giving ~5.4×10^{-10} cm^3 molecule^{-1} s^{-1} between 1950 and 2100 K. With updated equilibrium constants from active tables,[58] the transformed values for eq 35 then range between 62% and 75% of the values implied by eq 7, suggesting that reaction 35 may be the explanation for the excessively large [O] observed at long times in the experiments. We point out that this simple theory fails for eq −35 at lower temperatures, giving values ~6 times larger than those measured, probably because an entropy decrease is required in proceeding from a

collision complex to the H-bonded structure. This transformation may exhibit temperature dependence. Clearly, this reaction is quite complicated and will require new and more accurate determinations of the ab initio potential energy surface along with modern dynamical calculations to theoretically assess the *T*-dependence for eq 35 and its reverse over the entire range, 200 to 2150 K.

Implications to Methane Combustion

In the present study, new high-temperature values for four rate constants are deduced from both OH-radical and O-atom concentration profiles, that is, eqs 6, 7, 12, and 16. If these values are included in the mechanism given in Table 2, the question arises as to whether this mechanism can be used to explain induction delay experiments in the branching chain oxidation of CH_4. Inspection of the table shows that nothing can occur without adding initiation processes. We have therefore investigated the effects of including two such reactions

$$CH_4 + Kr \rightarrow CH_3 + H + Kr \qquad (18)$$

and

$$CH_4 + O_2 \rightarrow CH_3 + HO_2 \qquad (19)$$

with eq 18 already being well-known.[64] HO_2 in eq 19 also gives H which can react with CH_4 giving $CH_3 + H_2$, and therefore, a competition exists between this reaction and the main branching reaction, $H + O_2 \rightarrow OH + O$. The $H + CH_4$ reaction is also well-known[64] and is now included in the mechanism.

Figure 12 shows three [OH] simulations at different temperatures starting with 0.5% CH_4 and 10% O_2 in rare gas at a total density of $\sim 1 \times 10^{19}$ molecules cm^{-3}. These conditions are similar to those used by Hwang et al.[5] who were careful to take boundary layer effects into account in determining total density and temperature.[7,8] It is clear from Figure 12 that the mechanism as presented does predict chain branching and is sufficient to test ignition delay experiments. We point out that the mechanism should only be used in the initial stages of reactions because it is not detailed enough to explain the chemistry occurring in the high conversion regime. Last, we have attempted to fit the $t_{1/4}$ values of Hwang et al.[5] with the complete mechanism. The only unspecified rate constant is that for reaction 19. We find some sensitivity for predicted induction times to the rate constant for reaction 19, and the Hwang et al. $t_{1/4}$ OH-data values can be predicted with k_{19} being about three times larger than the value recommended by Baulch et al.[28]

Acknowledgment. The authors want to thank Dr. A. F. Wagner for a thorough reading of the manuscript and valuable suggestions. We also thank Dr. J. P. Hessler for supplying a prepublication manuscript of his work and Dr. B. Ruscic for valuable discussions. This work was supported by the U.S. Department of Energy, Office of Basic Energy Sciences, Division of Chemical Sciences, Geosciences and Biosciences under Contract No. W-31-109-Eng-38.

References and Notes

(1) *NIST Chemical Kinetics Database*, NIST Standard Reference Database 17, Gaithersburg, MD, 2000.
(2) Zhu, R.; Hsu, C.-C.; Lin, M. C. *J. Chem. Phys.* **2001**, *115*, 195.
(3) Yu, C.-L.; Wang, C.; Frenklach, M. *J. Phys. Chem.* **1995**, *99*, 14377.
(4) Michael, J. V.; Kumaran, S. S.; Su, M.-C. *J. Phys. Chem. A* **1999**, *103*, 5942.
(5) Hwang, S. M.; Ryu, S.-O.; DeWitt, K. J.; Rabinowitz, M. J. *J. Phys. Chem. A* **1999**, *103*, 5949.
(6) Eiteneer, B.; Frenklach, M. *J. Phys. Chem. A* **2000**, *104*, 9797.
(7) Michael, J. V.; Kumaran, S. S.; Su, M.-C. *J. Phys. Chem. A* **2000**, *104*, 9800.
(8) Hwang, S. M.; Ryu, S.-O.; DeWitt, K. J.; Rabinowitz, M. J. *J. Phys. Chem. A* **2000**, *104*, 9803.
(9) Scire, J. J., Jr.; Yetter, R. A.; Dryer, F. L. *Int. J. Chem. Kinet.* **2001**, *33*, 75.
(10) Hessler, J. P. *18th Combustion Research Conference*, Chemical Sciences Division Office of Basic Energy Sciences, U.S. DOE, Tahoe City, CA, May, 1996; pp. 134−137. Hessler, J. P.; Du, H.; Wagner, A. F.; Ogren, P. J., private communication, 2004.
(11) Herbon, J. T.; Hanson, R. K.; Bowman, C. T.; Golden, D. M. *Proc. Combust. Inst.* **2004**, *30*, 955.
(12) Su, M.-C.; Kumaran, S. S.; Lim, K. P.; Michael, J. V. *Rev. Sci. Instrum.* **1995**, *66*, 4649.
(13) Su, M.-C.; Kumaran, S. S.; Lim, K. P.; Michael, J. V.; Wagner, A. F.; Harding, L. B.; Fang, D.-C. *J. Phys. Chem. A* **2002**, *106*, 8261.
(14) Srinivasan, N. K.; Su, M.-C.; Sutherland, J. W.; Michael, J. V. *J. Phys. Chem. A* **2005**, *109*, 1857.
(15) Michael, J. V. *Prog. Energy Combust. Sci.* **1992**, *18*, 327.
(16) Michael, J. V. In *Advances in Chemical Kinetics and Dynamics*; Barker, J. R., Ed.; JAI: Greenwich, 1992; Vol. I, pp 47−112, for original references.
(17) Michael, J. V.; Sutherland, J. W. *Int. J. Chem. Kinet.* **1986**, *18*, 409.
(18) Michael, J. V. *J. Chem. Phys.* **1989**, *90*, 189.
(19) Michael, J. V.; Fisher, J. R. In *Seventeenth International Symposium on Shock Waves and Shock Tubes*; Kim, Y. W., Ed.; AIP Conference Proceedings 208; American Institute of Physics: New York, 1990; pp 210−215.
(20) Su, M.-C.; Kumaran, S. S.; Lim, K. P.; Michael, J. V.; Wagner, A. F.; Dixon, D. A.; Kiefer, J. H.; DiFelice, J. *J. Phys. Chem.* **1996**, *100*, 15827.
(21) Kumaran, S. S.; Su, M.-C.; Michael, J. V. *Int. J. Chem. Kinet.* **1997**, *29*, 535.
(22) Tsang, W.; Hampson, R. F. *J. Phys. Chem. Ref. Data* **1986**, *15*, 1087.
(23) Du, H.; Hessler, J. P. *J. Chem. Phys.* **1992**, *96*, 1077.
(24) Ruscic, B.; Wagner, A. F.; Harding, L. B.; Asher, R. L.; Feller, D.; Dixon, D. A.; Peterson, K. A.; Song, Y.; Qian, X.; Ng, C. Y.; Liu, J.; Chen, W.; Schwenke, D. W. *J. Phys. Chem. A* **2002**, *106*, 2727.
(25) Herbon, J. T.; Hanson, R. K.; Golden, D. M.; Bowman, C. T. *Proc. Combust.* Inst. **2002**, *29*, 1201.
(26) Oldenborg, R. C.; Loge, G. W.; Harridine, D. M.; Winn, K. R. *J. Phys. Chem.* **1992**, *96*, 8426.
(27) Wooldridge, M. S.; Hanson, R. K.; Bowman, C. T. *Int. J. Chem. Kinet.* **1994**, *26*, 389.
(28) Baulch, D. L.; Cobos, C. J.; Cox, R. A.; Esser, C.; Frank, P.; Just, Th.; Kerr, J. A.; Pilling, M. J.; Troe, J.; Walker, R. W.; Warnatz, J. *J. Phys. Chem. Ref. Data* **1992**, *21*, 411.
(29) Krasnoperov, L. N.; Chesnokov, E. N.; Stark, H.; Ravishankara, A. R. *J. Phys. Chem. A* **2004**, *108*, 11526.
(30) Timonen, R. S.; Ratajczak, E.; Gutman, D. *J. Phys. Chem.* **1988**, *92*, 651.
(31) Michael, J. V.; Su, M.-C.; Sutherland, J. W.; Carroll, J. J.; Wagner, A. F. *J. Phys. Chem. A* **2002**, *106*, 5297.
(32) Kumaran, S. S.; Carroll, J. J.; Michael, J. V. *Proc. Combust. Inst.* **1998**, *27*, 125.
(33) Davidson, D. F.; Di Rosa, M. D.; Chang, A. Y.; Hanson, R. K.; Bowman, C. T. *Proc. Combust. Inst.* **1992**, *24*, 589. Davidson, D. F.; Hanson, R. K.; Bowman, C. T. *Int. J. Chem. Kinet.* **1995**, *27*, 305.
(34) Walter, D.; Grotheer, H.-H.; Davies, J. W.; Pilling, M. J.; Wagner, A. F. *Proc. Combust.* Inst. **1990**, *23*, 107.
(35) Hwang, S. M.; Rabinowitz, M. J.; Gardiner, W. C., Jr. *Chem. Phys. Lett.* **1993**, *205*, 157.
(36) Lim, K. P.; Michael, J. V. *Proc. Combust. Inst.* **1994**, *25*, 713.
(37) Michael, J. V.; Keil, D. G.; Klemm, R. B. *Int. J. Chem. Kinet.* **1983**, *15*, 705.
(38) Tully, F. P. *Chem. Phys. Lett.* **1988**, *143*, 510.
(39) Lim, K. P.; Michael, J. V. *J. Chem. Phys.* **1993**, *98*, 3919.
(40) Fockenberg, C.; Hall, G. E.; Preses, J. M.; Sears, T. J.; Muckerman, J. T. *J. Phys. Chem. A* **1999**, *103*, 5722. Preses, J. M.; Fockenberg, C.; Flynn, G. W. *J. Phys.* Chem. A **2000**, *104*, 6758.
(41) Krasnoperov, L. N.; Michael, J. V. *J. Phys. Chem. A* **2004**, *108*, 8317.
(42) Langford, A. O.; Petek, H.; Moore, C. B. *J. Chem. Phys*. **1983**, *78*, 6650.
(43) Hancock, G.; Heal, M. R. *J. Phys. Chem.* **1992**, *96*, 10316.
(44) Hancock, G.; Haverd, V. *Chem. Phys. Lett*. **2003**, *372*, 288.
(45) Blitz, M. A.; McKee, K. W.; Pilling, M. J.; Seakins, P. W. *Chem. Phys. Lett*. **2003**, *372*, 295.
(46) Dombrowsky, Ch.; Wagner, H. Gg. *Ber. Bunsen-Ges. Phys. Chem*. **1992**, *96*, 1048.

(47) Baulch, D. L.; Cobos, C. J.; Cox, R. A.; Frank, P.; Hayman, G.; Just, Th.; Kerr, J. A.; Murrells, T.; Pilling, M. J.; Troe, J.; Walker, R. W.; Warnatz, J. *J. Phys. Chem. Ref. Data* **1994**, *23*, 847.

(48) Gonzalez, C.; Theisen, J.; Schlegel, H. B.; Hase, W. L.; Kaiser, E. W. *J. Phys. Chem.* **1992**, *96*, 1767.

(49) Krasnoperov, L. N.; Michael, J. V. *J. Phys. Chem. A* **2004**, *108*, 5643.

(50) Tsang, W. *J. Phys. Chem. Ref. Data* **1987**, *16*, 471.

(51) Michael, J. V.; Sutherland, J. W.; Harding, L. B.; Wagner, A. F. *Proc. Combust. Inst.* **2000**, *28*, 1471.

(52) http://www.me.berkeley.edu/gri_mech-3.0/.

(53) http://chem.leeds.ac.uk/combustion/combustion.html-1.5/.

(54) Zellner, R.; Ewig, F. *J. Phys. Chem.* **1988**, *92*, 2971.

(55) (a) Braun-Unkhoff, M.; Naumann, C.; Frank, P. In *Proceedings of the 19th International Symposium on Shock Waves*; Brun, R., Dumitrescu, L. Z., Eds.; Springer-Verlag: Berlin, 1995; Vol. 2, pp 203−208. (b) Naumann, C. In *Reaktionen von Methyl mit Sauerstoff und Stickstoffmonoxid und die O_2 Vibrationsrelaxation bei Verbrennungsrelevanten Temperaturen*; Ph.D. Dissertation, Universität Stuttgart, 1998, Göttingen: Cuvillier, 1999; with (b) apparently superseding (a).

(56) VonDrasek, W. A.; Okajima, S.; Kiefer, J. H.; Ogren, P. J.; Hessler, J. P. *Appl. Optics* **1990**, *29*, 4899.

(57) Walch, S. P. *Chem. Phys. Lett.* **1993**, *215*, 81.

(58) Ruscic, B.; Boggs, J. E.; Burcat, A.; Csaszar, A. G.; Demaison, J.; Janoschek, R.; Martin, J. M. L.; Morton, M. L.; Rossi, M. J.; Stanton, J. F.; Szalay, P. G.; Westmoreland, P. R.; Zabel, F.; Berces, T. *J. Phys. Chem. Ref. Data*, in press.

(59) Ruscic, B., private communication of results based on Active Thermochemical Tables v. 1.25 operating on the Core (Argonne) Thermochemical Network v. 1.045, for CH_3 and CH_3O, Jan., 2005. Ruscic, B.; Pinzon, R. E.; Morton, M. L.; von Laszevski, G.; Bittner, S. J.; Nijsure, S. G.; Amin, K. A.; Minkoff, M.; Wagner, A. F. *J. Phys. Chem. A* **2004**, *108*, 9979, for O-atoms.

(60) Michael, J. V.; Su, M.-C.; Sutherland, J. W.; Fang, D.-C.; Harding, L. B.; Wagner, A. F.; Maity, D. K.; Lin, D.; Tirtowidjojo, M.; Truong, T. N. *J. Phys. Chem. A*, in preparation.

(61) Dupuis, M.; Fitzgerald, G.; Hammond, B.; Lester, W. A., Jr.; Schaefer, H. F. *J. Chem. Phys.* **1986**, *84*, 2691.

(62) Varandas, A. J. C.; Yu, H. G. *Molecular Physics* **1997**, *91*, 301 and references therein.

(63) Su, M.-C.; Michael, J. V. *Proc. Combust. Inst.* **2002**, *29*, 1219.

(64) Sutherland, J. W.; Su, M.-C.; Michael, J. V. *Int. J. Chem. Kinet.* **2001**, *33*, 669.